Available online at www.sciencedirect.com
SCIENCE DIRECT®
Earth and Planetary Science Letters 241 (2006) 47–64
EPSL
www.elsevier.com/locate/epsl

Os–Hf–Sr–Nd isotope and PGE systematics of spinel peridotite xenoliths from Tok, SE Siberian craton: Effects of pervasive metasomatism in shallow refractory mantle

Dmitri A. Ionov [a,b,c,*], Steven B. Shirey [d], Dominique Weis [b,e], Gerhard Brügmann [a]

[a] *Max-Planck-Institut für Chemie, Postfach 3060, D-55020 Mainz, Germany*
[b] *Department of Earth and Environmental Sciences, Université Libre de Bruxelles, Brussels 1050, Belgium*
[c] *Institut fuer Mineralogie, J.W. Goethe-Universitaet, Postfach 111932, 60054 Frankfurt/Main, Germany*
[d] *Department of Terrestrial Magnetism, Carnegie Institution of Washington, 5241 Broad Branch Road, NW Washington, DC 20015 USA*
[e] *EOS, University of British Columbia, Vancouver, Canada, V6T 1Z4*

Received 25 July 2005; received in revised form 31 October 2005; accepted 31 October 2005
Available online 1 December 2005
Editor: K. Farley

Abstract

Os–Hf–Sr–Nd isotopes and PGE were determined in peridotite xenoliths carried to the surface by Quaternary alkali basaltic magmas in the Tokinsky Stanovik Range on the Aldan shield. These data constrain the timing and nature of partial melting and metasomatism in the lithospheric mantle beneath SE Siberian craton. The xenoliths range from the rare fertile spinel lherzolites to the more abundant, strongly metasomatised olivine-rich (70–84%) rocks. Hf–Sr–Nd isotope compositions of the xenoliths are mainly within the fields of oceanic basalts. Most metasomatised xenoliths have lower $^{143}Nd/^{144}Nd$ and $^{176}Hf/^{177}Hf$ and higher $^{87}Sr/^{86}Sr$ than the host basalts indicating that the metasomatism is older and has distinct sources. A few xenoliths have elevated $^{176}Hf/^{177}Hf$ (up to 0.2838) and plot above the Hf–Nd mantle array defined by oceanic basalts.

$^{187}Os/^{188}Os$ in the poorly metasomatised, fertile to moderately refractory ($Al_2O_3 \geq 1.6\%$) Tok peridotites range from 0.1156 to 0.1282, with oldest rhenium depletion ages being about 2 Ga. The $^{187}Os/^{188}Os$ in these rocks show good correlations with partial melting indices (e.g. Al_2O_3, modal cpx); the intercept of the Al–$^{187}Os/^{188}Os$ correlation with lowest Al_2O_3 estimates for melting residues (~0.3–0.5%) has a $^{187}Os/^{188}Os$ of ~0.109 suggesting that these peridotites may have experienced melt extraction as early as 2.8 Gy ago. $^{187}Os/^{188}Os$ in the strongly metasomatised, olivine-rich xenoliths (0.6–1.3% Al_2O_3) ranges from 0.1164 to 0.1275 and shows no apparent links to modal or chemical compositions. Convex-upward REE patterns and high abundances of heavy to middle REE in these refractory rocks indicate equilibration with evolved silicate melts at high melt/rock ratios, which may have also variably elevated their $^{187}Os/^{188}Os$. This inference is supported by enrichments in Pd and Pt on chondrite-normalised PGE abundance patterns in some of the rocks. The melt extraction ages for the Tok suite of 2.0 to 2.8 Ga are younger than oldest Os ages reported for central Siberian craton, but they must be considered minimum estimates because of the extensive metasomatism of the most refractory Tok peridotites. This metasomatism could have occurred in the late Mesozoic to early Cenozoic when the Tok region was close to the subduction-related Pacific margin of Siberia and experienced large-scale

* Corresponding author. Institut fuer Mineralogie, J.W. Goethe-Universitaet, Postfach 111932, 60054 Frankfurt/Main, Germany. Tel.: +49 69798 25183.
E-mail address: ionov@em.uni-frankfurt.de (D.A. Ionov).

0012-821X/$ - see front matter
doi:10.1016/j.epsl.2005.10.038

tectonic and magmatic activity. This study indicates that metasomatic effects on the Re–Os system in the shallow lithospheric mantle can be dramatic.

Keywords: Siberia; mantle peridotite; metasomatism; Os isotopes; Hf–Nd–Sr isotopes; PGE

1. Introduction

Constraints on the age of continental lithospheric mantle (CLM) domains, their history and the way the lithosphere evolves can be provided by Re–Os isotopes in concert with other radiogenic isotopic systems (e.g. Sr, Nd, Hf) and trace elements. Of particular interest are such data on cratonic peridotites, which represent the most ancient CLM. Important insights into the early history of cratonic domains in South Africa and North America have been gained recently through studies of Re–Os and other isotope systems in peridotite xenoliths from those regions ([1], refs therein). By contrast, the CLM of the Siberian craton remains poorly studied. The only suite of mantle peridotites from the Siberian craton, for which a large set of Os, Sr and Nd isotope data is currently available, comes from the Udachnaya kimberlite in central craton [2,3] (Fig. 1). A small number of Sr–Nd isotope data and one Os isotope analysis have been provided also for peridotite xenoliths from the Mir pipe [2,3]; no Hf isotope data have been published as yet. Importantly, the published data on xenoliths from the Siberian kimberlites only characterize the CLM within the sub-longitudal belt of kimberlite fields in the central and northern parts of the craton (Fig. 1) while information on the CLM along its southern margin remains very scarce.

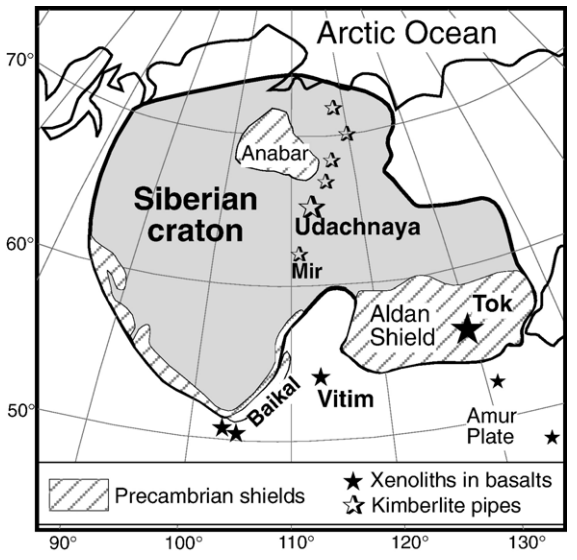

Fig. 1. A sketch map of the Siberian craton and adjacent regions (modified from [68]).

Petrography and chemical compositions have been recently provided for spinel peridotite xenoliths in alkali basaltic rocks in the Tokinsky Stanovik Range near the southern rim of the Aldan shield (referred to as Tok below) [4–6]. These are the only currently available samples of the CLM in the south-eastern (SE) Siberian craton and also the only known suite of mantle peridotites in Cenozoic basalts on the craton. The xenoliths from Tok are large and fairly fresh (in particular compared to strongly altered kimberlite-hosted xenoliths) and hence yield excellent material for studies of both whole-rock samples and mineral separates. This paper presents Os–Hf–Sr–Nd isotope and PGE data for the same samples (Table 1), which were a subject of detailed petrographic and chemical studies [4–6].

The goal of this paper is to characterize the radiogenic isotope composition of the CLM in the SE Siberian craton, give more insights into the origin and the evolution of the CLM in north-eastern Asia and outline links between the mantle events and the geologic history. In particular, the aim is to provide the first age estimates for the CLM beneath the SE Siberian craton and thus to better constrain the timing of the assembly of the craton and its relationships with the off-craton CLM in the nearby southern Siberia and Mongolia. Another major objective is to explore the effects of metasomatism on PGE and Os isotope compositions of mantle peridotites, which only have been broadly discussed recently [7–13], in further detail. This is especially possible with the Tok suite because recent petrographic and chemical studies show that many Tok peridotites are strongly metasomatised and show the effects of several enrichment processes [5,6].

2. Samples and analytical methods

The xenoliths for this study were found among massive lava fragments and show little effects of surface alteration (Figs. 2 and 3 in [4]). Clean rock chips or slabs cut from central parts of xenoliths were broken to yield 150–1100 g of crushed material free of metal

Table 1
Sample list with a summary of modal data, Mg# in olivine and *T* estimates

Sa.N°	Rock type	Al_2O_3 wt%	Mg# ol	Modal abundances wt.% ol	opx	cpx	*T* °C Ca-opx	Os is.	PGE	Hf is.	Sr is.	Nd is.
Lherzolite–harzburgite (LH) series peridotites												
1-2	Harzburgite	0.63	0.913	79	17	3	910	+				
1-13	Harzburgite	0.88	0.910*	80	16	3	933			+		+
2-6	Low-cpx lh.	1.25	0.899*	67	25	6	980	+	+			
2-9	Harzburgite	0.76	0.914	79	16	3	874	+				
3-4	Harzburgite	1.10	0.910*	74	21	3	910	+				
3-19	Low-cpx lh.	1.30	0.900*	70	21	6	931	+	+			
5-3	Lherzolite	1.25	0.904	74	15	9	907	+	+			
6-1	Lherzolite	3.94	0.895	55	26	17	1010	+		+	+	+
6-2	Lherzolite	3.98	0.895	54	26	17	1001	+		+	+	+
6-3	Lherzolite	2.47	0.909*	55	33	10	976	+		+	+	+
7-1	Low-cpx lh.	0.82	0.911	79	15	5	985			+	+	+
7-5	Lherzolite	3.34	0.901	57	26	14	985	+		+	+	
8-1	Low-cpx lh.	1.64	0.904*	74	17	7	1005	+		+	+	+
8-2	Low-cpx lh.	1.26	0.906	74	19	6	976	+				
8-5	Lherzolite	2.60	0.901*	63	24	10	1004	+		+	+	+
8-6	Lherzolite	3.58	0.896*	59	23	15	985	+	+	+	+	+
8-11	Harzburgite	0.75	0.913	78	17	5	957	+		+	+	+
8-31	Harzburgite	1.11	0.916	76	17	5	887	+	+			
8-39	Lherzolite	3.92	0.894	54	26	17	964	+		+	+	+
8-40	Harzburgite	0.86	0.913	71	24	4	922	+	+			
8-50	Harzburgite	1.14	0.912	77	18	4	992	+		+	+	+
10-2	Harzburgite	0.80	0.915	77	17	4	914	+				
10-4	Harzburgite	0.77	0.914	80	16	3	926	+				
10-8	Harzburgite	0.79	0.908	79	15	5	950			+		+
10-16	Low-cpx lh.	0.90	0.899*	76	17	6	957			+		+
10-17	Harzburgite	1.64	0.907	76	19	4	1011	+		+	+	+
10-19	Harzburgite	0.89	0.911	73	23	3	951	+		+	+	+
Lherzolite–wehrlite (LW) series peridotites												
8-10	Wehrlite	2.03	0.877	79	1	17	984	+				
10-3	Wehrlite	0.76	0.842	84	–	16	982	+	+			
Olivine–cpx cumulate												
8-14	Ol–cpx cumul	6.55	0.805					+		+	+	+

Data are from Ionov et al. [4,5]; collection year is omitted in sample numbers. Wr, whole-rock; ol, olivine; opx, orthopyroxene; cpx, clinopyroxene. *T* estimates are after [74]. Mg#, $Mg/(Mg+Fe)_{at}$; (*) heterogeneous olivine (1σ/mean > 1% for FeO and > 0.1% for Mg#).

chips. Split aliquots were ground in agate jars to fine powder. Detailed information on sample selection and handling is given in [4] and in Supplementary file. Table 1 gives a summary of modal compositions, temperature (*T*) estimates, whole-rock Al_2O_3 contents and $Mg\#_{ol}$ [$Mg/(Mg+Fe)_{at}$ in olivine].

Os isotope compositions and Re and Os abundances were determined at DTM and MPI by negative thermal ionisation mass spectrometry (N-TIMS). Abundances of Ir, Ru, Pd and Pt were determined using isotope dilution and multiple-collector inductively coupled MS (MC-ICPMS) at MPI. Hf–Sr–Nd isotope analyses were done at ULB using MC-ICPMS and TIMS. Detailed information on the analytical methods is given in Supplementary file.

3. Summary of petrography and chemical compositions

Ionov et al. [4,5] identified three rock series among Tok peridotites based on petrography and Mg# (Table 1). (1) The lherzolite–harzburgite (LH) series has 'normal' Mg# (0.89–0.92) and modal abundances of olivine (54–80%), orthopyroxene (opx, 15–33%) and clinopyroxene (cpx, 3–17%). It groups together fertile (cpx-rich lherzolite) to refractory (harzburgite) rocks, the latter being the most common (Table 1). (2) The lherzolite–wehrlite (LW) series peridotites make up about a quarter of Tok xenoliths; they have high modal olivine (66–84%) but lower Mg# (0.83–0.89) and much lower modal opx (0–12%) than the LH

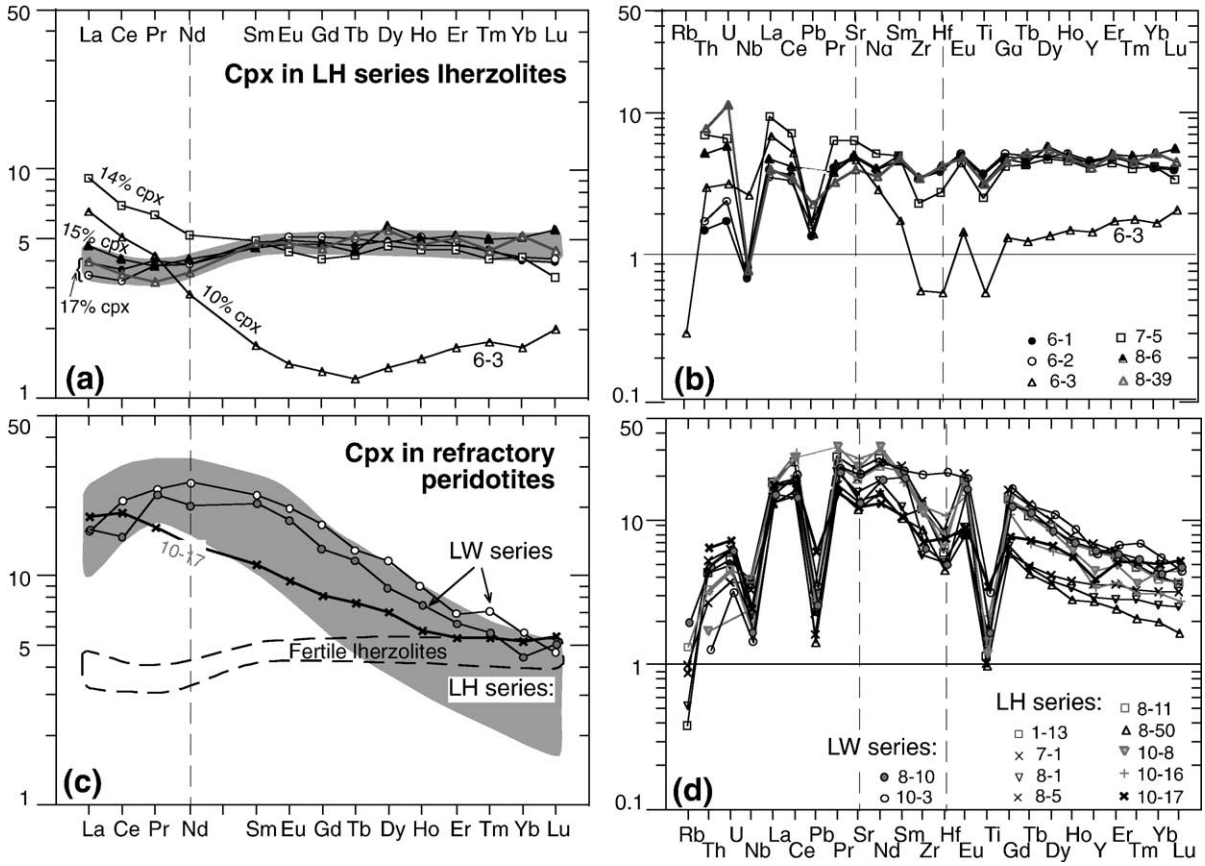

Fig. 2. (a–d) Primitive mantle-normalised [69] REE (left column) and multi-element (right column) abundance patterns of cpx in Tok xenoliths [6]. Note increasing LREE-enrichments at lower modal cpx (a) and similar patterns (e.g. $La/Sm_{PM}<1$; $Sm/Yb_{PM} \gg 1$) for cpx in the majority of refractory samples (c–d).

rocks. Ionov et al. [4] considered the LH series to be residues of shallow partial melting whereas the LW series results from reactive percolation of evolved under-saturated silicate melts through refractory partial melting residues [5]. Such melt percolation involves Fe-enrichment and widespread replacement of opx by cpx. (3) The least abundant among Tok xenoliths are olivine–cpx cumulates; their Mg# (0.79–0.84) are generally lower than for the LW series.

Many LW series and refractory LH series Tok xenoliths have accessory amphibole, phlogopite and/or fine-grained interstitial materials; the latter contain phosphates, alkali feldspar, Ti-rich oxides and other rare minerals. These minerals may have formed due to fractional crystallisation of trapped percolating melts and late-stage fluids [6]. The cpx in the Tok peridotites commonly has high contents of Na_2O and Cr_2O_3; some xenoliths (e.g. 10–19) contain cpx generations with different Na_2O contents [4,6].

Trace element compositions of the cpx (determined by LA-ICPMS) and of whole-rocks (determined by solution ICPMS) were reported by Ionov et al. [6]. Cpx in fertile LH series peridotites (with 15–17% cpx) has nearly flat REE patterns, with a fairly narrow range of primitive mantle-normalised abundances ($REE_{PM}=3$–5), minor La and La–Ce inflections and small positive Sr anomalies (Fig. 2a). REE patterns of the cpx in moderately refractory (6–14% cpx) LH series lherzolites are LREE-enriched ($La/Nd_{PM}>1$; $Nd/Yb_{PM}>1$). The shapes of the patterns change in concert with modal compositions such that the lherzolites with less cpx have increasingly higher abundances of LREE, MREE and Sr in the cpx (Fig. 2a–b). Cpx in nearly all refractory (>70% olivine) peridotites, including both LH and LW series rocks, has convex-upward REE patterns ($La/Nd_{PM}<1$; $Nd/Yb_{PM} \gg 1$), with a relatively narrow LREE–MREE abundance range, a fairly broad HREE range and $Sr/Nd_{PM}<1$ (Fig. 2c–d). Cpx in LH series harzburgite 10-17 has the least fractionated REE pattern with relatively high HREE and low MREE (Fig. 2d).

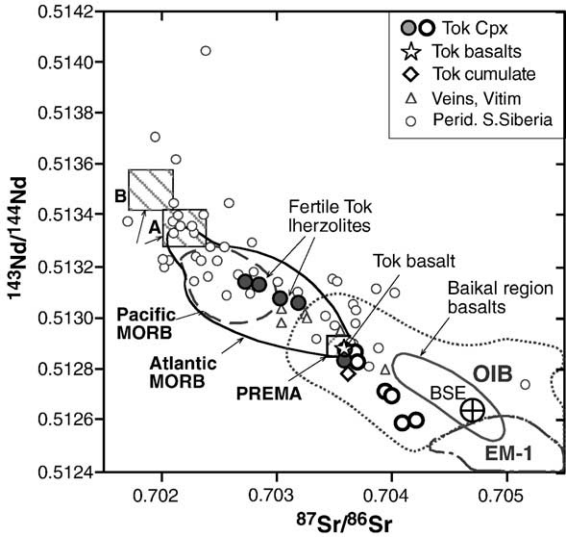

Fig. 3. Plot of $^{87}Sr/^{86}Sr$ vs. $^{143}Nd/^{144}Nd$ for cpx in LH series Tok xenoliths. Filled circles, poorly to moderately metasomatised cpx; empty circles, strongly metasomatised cpx with convex-upward REE patterns (Fig. 2). Also shown are peridotite xenoliths from the Baikal region [16] and SE Siberia [23]; calculated whole-rock values are shown for Vitim garnet peridotites, cpx analyses are shown for other xenoliths. Fields of mid-ocean-ridge basalts (MORB), ocean island basalts (OIB) and enriched mantle (EM-1) are after [20]; bulk silicate Earth (BSE), prevalent mantle (PREMA) and depleted mantle (DMM A and B) are after [19].

For the purpose of the discussion below, we identify two groups of Tok xenoliths based on their REE patterns: (1) poorly to moderately metasomatised and (2) strongly metasomatised. The first one groups xenoliths with LREE-depleted to LREE-enriched ($La/Nd_{PM}>1$) cpx; it includes the LH series lherzolites (10–17% cpx) and harzburgite 10-17 (Fig. 2). The second group has cpx with convex-upward REE patterns ($La/Nd_{PM}<1$; $Nd/Yb_{PM} \gg 1$); all those xenoliths are refractory. The first type of pattern can be produced by relatively small additions of LREE-enriched fluids to LREE-depleted melting residues whereas the convex-upward patterns indicate high degrees of equilibration with such fluids ([14,15], refs. therein). Importantly, the latter type of metasomatism implies open-system percolation processes with high melt/rock ratios.

Cpx in all LH series peridotites has negative anomalies of Hf and other high-field-strength elements (HFSE) relative to adjacent REE; these anomalies tend to be deeper in cpx from refractory rocks (Fig. 2). Nevertheless, the cpx in all olivine-rich xenoliths has $HREE/Hf_{PM}<1$, which indicates that the abundances of Hf (less compatible than HREE), as well as those of LREE–MREE, in the LH series cpx have been affected by metasomatism. Only one Tok xenolith (lherzolite 6-3) has cpx with $Lu/Hf_{PM} \gg 1$ (Fig. 2b).

Fertile Tok peridotites have spoon-shape whole-rock REE patterns with minor LREE-enrichments, like their cpx [4,6]. The REE patterns of refractory Tok peridotites usually are fractionated, with LREE>MREE>HREE. The majority of LH series rocks have La-enriched ($La/Nd_{PM}>1$) or flat LREE patterns, which are commonly distinct from those in their cpx ($La/Nd_{PM}<1$) because a significant proportion of LREE in those rocks resides in inter-granular material, e.g. phosphates [6]. Cumulate 8-14 has a fairly smooth convex-upward pattern, with higher HREE, MREE, Y, Sr, Ti, Zr, Hf and Pb than in the LH and LW xenoliths.

4. Results

4.1. Hf–Sr–Nd isotope compositions

Hf–Sr–Nd isotope compositions for Tok xenoliths and host basalts obtained in this study are given in Table 2 together with abundances of Lu, Hf, Sm, Nd and Sr after [6]. Hf–Sr–Nd isotope compositions of the cpx separates obtained in this study are assumed to be representative of those for the whole-rock xenoliths prior to incorporation in the host basalt. This assumption is almost certainly true for poorly metasomatised, cpx-rich (14–17%) peridotites because the cpx in such rocks is by far the most important mineral host for Hf, Sr and Nd (e.g. [16,17]). On the other hand, significant proportions of Sr and Nd in strongly metasomatised, refractory Tok peridotites may be hosted by accessory phosphates, while opx and interstitial Ti-rich oxides may host much Hf [6]. If the cpx in such peridotites are in isotopic equilibrium with the co-existing minerals in the Tok mantle, strong isotope disequilibrium is not likely to have developed after the xenoliths were transported to the surface because the host volcanic rocks are young (0.3–0.6 Ma) [18].

Sr–Nd isotope compositions of all the Tok xenoliths (Table 2; Fig. 3) fall within the range of oceanic basalts [19,20]. Fertile Tok lherzolites plot in the middle of the Atlantic MORB field while refractory peridotites and the ol–cpx cumulate fall within the OIB field between the bulk silicate earth (BSE) and the PREMA model composition after [19]. Alkali basaltic rocks hosting the xenoliths have higher $^{143}Nd/^{144}Nd$ and lower $^{87}Sr/^{86}Sr$ than those from nearby Baikal rift zone [21,22] and overlap the PREMA. Strongly metasomatised Tok xenoliths have lower $^{143}Nd/^{144}Nd$ and higher $^{87}Sr/^{86}Sr$ than their host basalts. Many Tok xenoliths

Table 2
Hf–Nd–Sr isotope compositions and Lu, Hf, Sr, Nd and Sm abundances in Tok xenoliths

Sample N°	Weight (g)	Nu Plasma MC-ICPMS				TIMS				Abundances, ppm				
		$^{176}Hf/^{177}Hf$	$2\sigma \times 10^{-6}$	$^{143}Nd/^{144}Nd$	$2\sigma \times 10^{-6}$	$^{143}Nd/^{144}Nd$	$2\sigma \times 10^{-6}$	$^{87}Sr/^{86}Sr$	$2\sigma \times 10^{-6}$	Lu	Hf	Sm	Nd	Sr
Tok, whole-rocks														
8-14cumul	0.270	0.283097	11	0.512801	4	0.512781	11	0.703600	10	0.11	1.6	2.7	9.4	120
8-1bas	0.101	0.283088	11			0.512883	12			0.22	5.3	8.0	41	1089
8-1bas*	0.1					0.512882	5	0.703559	6					
Stk51bas*	0.1					0.512884	6	0.703595	5	0.22	3.9	7.6	41	1036
Tok, LH series clinopyroxenes														
1-13	0.195	0.283073	8	0.512855	6	0.512858	11			0.23	1.6	8.2	31	399
6-1	0.322	0.283232	11			0.513083	10	0.702998	7	0.25	1.0	1.9	4.6	87
6-2	0.383	0.283153	10	0.513147	4	0.513130	9	0.702822	8	0.26	1.1	1.8	4.6	87
6-3	0.683	0.283793	9	0.512883	5	0.512870	8	0.703574	7	0.14	0.15	0.7	3.5	85
6-3dupl	0.30			0.512880	3	0.512884	7	0.703581	6					
7-1	0.199	0.283040	8			0.512865	8	0.703619	7	0.24	2.3	9.1	29	348
7-5	0.353	0.283369	12	0.513056	9	0.513058	19			0.22	0.7	1.9	6.1	112
8-1	0.298	0.283042	14	0.512727	4	0.512712	10	0.703919	6	0.16	1.4	4.8	22	281
8-5av.2	0.212	0.283123	13			0.512600	9	0.704191	7	0.21	2.1	4.1	18	247
8-6	0.274	0.283325	11	0.513085	4	0.513065	8	0.703145	7	0.26	1.1	1.8	4.8	90
8-6dupl						0.513048	22	0.703095	6					
8-11	0.232	0.283080	12			0.512843	7	0.703619	7	0.24	1.7	8.2	27	344
8-11dupl								0.703630	7					
8-39	0.306	0.283266	10			0.513144	9	0.702696	6	0.29	1.2	1.9	4.3	73
8-50	0.288	0.282939	8			0.512590	8	0.704053	7	0.11	1.2	4.0	19	219
10-8	0.193	0.283014	10	0.512839	8	0.512835	13			0.29	2.1	7.9	39	431
10-16	0.147	0.283137	16	0.512894	8	0.512911	12			0.18	3.0	7.1	36	497
10-17	0.220	0.283076	13	0.512876	4	0.512840	9	0.703545	7	0.34	2.1	4.3	16	228
10-19	0.232	0.282837	11	0.512736	4	0.512698	8	0.703945	7	0.10	1.8	3.6	23	252

Cumul, cumulate; bas, basalt. The errors for the isotope measurements are 2σ in-run statistics. Element abundances are after [6].
*Two basalt samples marked with asterisks were analysed at Vancouver.

plot on the Sr–Nd isotope diagram close to metasomatised xenoliths from southern Siberia, e.g. veined xenoliths from Vitim. Several metasomatised Tok peridotites however yield lower $^{143}Nd/^{144}Nd$ (<0.51288) than any other mantle xenoliths reported from the region [16,23] (Fig. 3). None of the Tok xenoliths has highly depleted Sr and Nd isotope compositions similar to the DMM model end-member [19]. They are different in this regard from fertile xenoliths from the Vitim and other volcanic fields in southern Siberia [16,24].

$^{176}Hf/^{177}Hf$ in all Tok xenoliths but one range from 0.2828 to 0.2834, i.e. fall within the range of oceanic basalts ([17,25], refs. therein) (Fig. 4). Cpx 6-3 yielded a much higher value of 0.2838. Two Tok xenoliths (6-3 and 8-5) plot above the mantle Hf–Nd array defined by the basalt data because they have significantly higher epsilon Hf values at given epsilon Nd than the oceanic basalts (Fig. 4a). Xenoliths with similar Hf–Nd isotope relationships were earlier reported from Vitim [17], Nikos kimberlite in Canada [26] (Fig. 4a) and other mantle peridotite series [1,27,28], but their proportion in the Tok suite is relatively small compared to these other localities.

4.2. Re and PGE abundances

Re and Os abundances and Os isotope compositions in the Tok xenoliths are given in Table 3. The Os abundances range from 1 to 4 ppb except for sample 8-31, which contains as little as 0.1 ppb Os (confirmed by a duplicate analysis) (Fig. 5). This concentration range is similar to that reported for peridotite xenoliths from the Udachnaya kimberlite in the central Siberian craton [2] although the frequency distribution of Os values in the two suites is different, e.g. the Tok suite has a higher proportion of Os-rich (3–4 ppb) rocks (Fig. 5b inset). Os abundances in the Tok suite are markedly higher than in Vitim peridotites, the only other xenolith series from southern Siberia, for which Re–Os data are currently available [12]. In general, Os abundances in the Tok xenoliths do not show regular correlations with Al_2O_3 or other partial melting indices (Fig. 5a). However, it is evident from Fig. 5a that the majority (75%) of Al-poor ($2.6\% < Al_2O_3$) Tok peridotites contain more Os (2–4 ppb) than fertile Tok peridotites (0.9–1.8 ppb Os).

Re abundances in the Tok xenoliths are very low (0.001–0.065 ppb), i.e. are similar to or even lower than

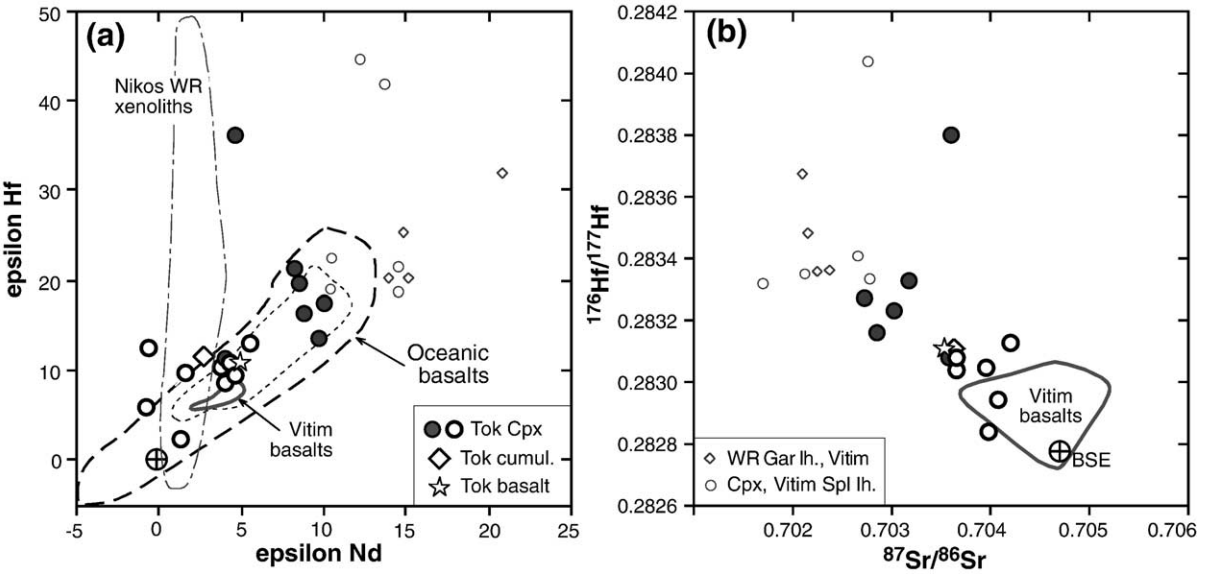

Fig. 4. Plots of $^{143}Nd/^{144}Nd$ (a) and $^{87}Sr/^{86}Sr$ (b) vs. $^{176}Hf/^{177}Hf$ for Tok xenoliths; symbols are the same as in Fig. 3. Also shown are xenoliths from Vitim [16,17] and fields for MORB and OIB (outlined after a compilation of published data by J. Blichert-Toft shown in Fig. 8 of [17]), Vitim basalts [22] and xenoliths from Nikos kimberlite in Canada [26].

in the Vitim peridotites (Fig. 5b). In particular, fertile Tok lherzolites contain as little as 0.04–0.065 ppb Re, that is much lower than estimated for primitive mantle (PM, 0.28 ppb; [29]). Much higher Re abundances were found in many Udachnaya peridotites (Fig. 5b inset) but it is not clear to what extent the high Re in those strongly altered, kimberlite-hosted xenoliths results from Re enrichments during and after their transport to the surface [1,2]. Overall, the Re and Os abundances in the Tok xenoliths do not appear to be correlated (Fig. 5b inset). However, if three refractory xenoliths with lowest Os are discarded, the remainder of the samples outline a trend of lower Re at higher Os. Although Re abundances in the Tok xenoliths are positively correlated with Al_2O_3 (Fig. 5b), possible interpretations of that fairly rough trend in terms of partial melting relationships are compromised by the very low Re in the fertile peridotites. Re and Os abundances in two LW series peridotites (wehrlites) analysed do not differ from those in olivine-rich LH series Tok xenoliths (Fig. 5).

PGE abundances in seven Tok xenoliths are given in Table 4; their chondrite-normalised patterns are shown in Fig. 6. Apart from sample 8-31 (which has anomalously low Os, Ir and Ru), the Tok peridotites have similar abundances of Ir and Ru. Fertile lherzolite 8–6 has low Os/Ir (Table 4; Fig. 6), like peridotite xenoliths from Vitim [12] and some other off-craton suites [30,31]. By contrast, five olivine-rich Tok xenoliths have nearly flat patterns of iridium-group PGE (Ir, Os, Ru; I-PGE). The concentration range of Pt and Pd, while roughly centred about the same chondrite-normalised abundance, is much broader than for I-PGE, and the Ru–Pt–Pd relationships are quite complex (Fig. 6). Three samples have smooth and consistent Ru–Pt–Pd patterns; two of them (2–6 and 5–3) show moderate depletions in Pt and Pd relative to I-PGE, one (8–40) is enriched in Pt and Pd. The remaining three samples are enriched either in Pt or in Pd. These random enrichments distinguish the Tok xenoliths from many other refractory peridotite suites, in which chondrite-normalised abundances of Pt and Pd are commonly lower than those of I-PGE (e.g. [12,32]; Fig. 6).

PGE in mantle peridotites are commonly believed to reside mainly in sulfides [7,30,33–35]. Careful inspection of 1–3 high quality thin sections per sample under microscope in reflected and transmitted light found almost no sulfide grains bigger than 1–5 μm in the Tok xenoliths. Small quantities of tiny sulfides are occasionally found as arrays along cracks in minerals and in fine-grained interstitial materials. Such secondary sulfides are commonly low in Os [7] and hence are unlikely to be major Os carriers in the Tok peridotites; moreover, they were not found in all the xenoliths we studied.

4.3. Os isotope compositions

$^{187}Os/^{188}Os$ in the Tok peridotites range from 0.1156 to 0.1289 (Table 3). None of the 25 samples we analysed yielded very low $^{187}Os/^{188}Os$, like those

Table 3
Re and Os abundances and isotope ratios

Sa.N°	Os conc. ppb	$^{187}Os/^{188}Os$ blank-corr	2σ precision	Re conc. ppb	$^{187}Re/^{188}Os$
DTM analyses					
1-2	2.80	0.12334	0.00018	0.001	0.002
2-9	3.84	0.11900	0.00008	0.016	0.020
3-4	1.37	0.12128	0.00015	0.006	0.021
6-1	0.98	0.12817	0.00023	0.065	0.319
6-2	0.88	0.12789	0.00014	0.056	0.309
6-3	3.03	0.12205	0.00031	0.024	0.037
7-5	1.62	0.12645	0.00011	0.041	0.122
8-1	3.92	0.12544	0.00022	0.005	0.006
8-2	1.79	0.12371	0.00010	0.027	0.071
8-5	2.78	0.12219	0.00015	0.036	0.063
8-6	1.64	failed		0.052	0.154
$8\text{-}10^{LW}$	2.31	0.12433	0.00008	0.005	0.011
8-11	3.08	0.12331	0.00015	0.009	0.014
8-14	0.02	failed		0.034	7.18
8-31	0.08	0.12319	0.00041	0.001	0.001
8-39	1.36	0.12887	0.00009	0.057	0.202
8-50	3.25	0.12105	0.00010	0.019	0.028
10-2	1.74	0.11635	0.00007	0.023	0.063
10-4	0.94	0.12547	0.00018	0.001	0.003
10-17	2.20	0.11556	0.00012	0.024	0.053
10-19	3.34	0.12656	0.00007	0.005	0.007
MPI–Mainz analyses					
2-6	3.83	0.12751	0.00023	0.024	0.032
3-19	3.51	0.12013	0.00017	0.029	0.044
5-3	2.21	0.12598	0.00017	0.065	0.16
8-31	0.12	0.12235	0.00034	0.037	1.62
8-40	2.64	0.12274	0.00022	0.059	0.12
8-6	1.53	0.12559	0.00015	0.069	0.24
$10\text{-}3^{LW}$	3.04	0.12541	0.00017	0.021	0.037

LW, lherzolite–wehrlite series rocks.

found in some Udachnaya peridotites (0.108–0.114) [2]. One should note however that four out of five Udachnaya xenoliths with $^{187}Os/^{188}Os < 0.114$ are so-called megacrystalline dunites and harzburgites (Fig. 7), which probably come from the bottom of the cratonic keel. These rare rocks have very coarse grain size and contain Ca-poor, Cr-rich garnets; some are diamond-bearing. By contrast, the Tok xenoliths are shallow (40–60 km) spinel facies rocks. The most common $^{187}Os/^{188}Os$ values in both Tok and Udachnaya suites are 0.122–0.124. However, the Tok suite yielded a much higher proportion of relatively radiogenic $^{187}Os/^{188}Os$ (0.124–0.129) (Figs. 7 and 8a). To some extent, this may be due to a greater number of fertile xenoliths analysed in the Tok suite, but many olivine-rich Tok peridotites also have $^{187}Os/^{188}Os$ in that range.

$^{187}Os/^{188}Os$ in the Tok xenolith suite on the whole does not appear to be related to modal or major element compositions. In particular, the most refractory LH

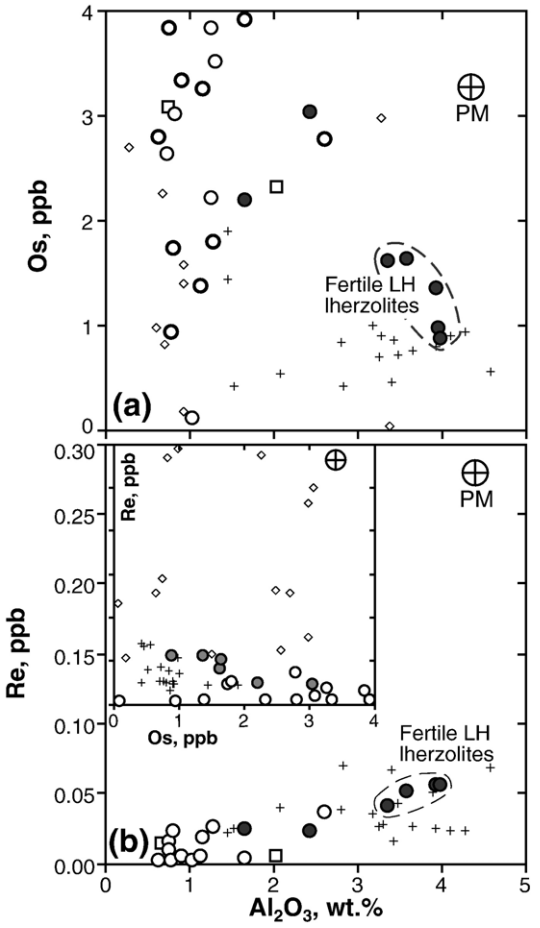

Fig. 5. Co-variation plots for Os (a) and Re (b) vs. Al_2O_3 in Tok xenoliths (symbols for LH series and cumulate are the same as in Fig. 3; squares, LW series). Also shown are peridotite xenoliths from Vitim (crosses, [12]) and Udachnaya (small rhombs, [2]). Primitive mantle (PM) is after [29]. Inset in (b) shows Re–Os co-variation.

series peridotites (0.6–1.3% Al_2O_3) yield $^{187}Os/^{188}Os$ variation range (0.1164 to 0.1275) nearly as broad as that for the whole suite (Fig. 8a). The two LW series samples analysed have relatively radiogenic $^{187}Os/^{188}Os$ values within that range (0.1243–0.1254)

Table 4
PGE abundances in Tok xenoliths (in ppb)

Sa. N°	Os	Ir	Ru	Pd	Pt	$(Pd/Ir)_N$	$(Os/Ir)_N$
2-6	3.83	2.77	4.81	1.29	4.54	0.4	1.3
3-19	3.51	3.24	5.50	0.68	14.2	0.2	1.0
5-3	2.21	2.58	3.84	2.14	5.43	0.7	0.8
8-6	1.53	2.68	3.64	5.35	3.30	1.6	0.5
8-31	0.12	0.23	1.59	1.47	n.d.	5	0.5
8-40	2.64	2.73	4.74	4.36	9.38	1.3	0.9
10-3	3.04	2.70	5.34	4.86	2.65	1.5	1.1

N, normalised to primitive mantle Ref. [37].
n.d., not determined.

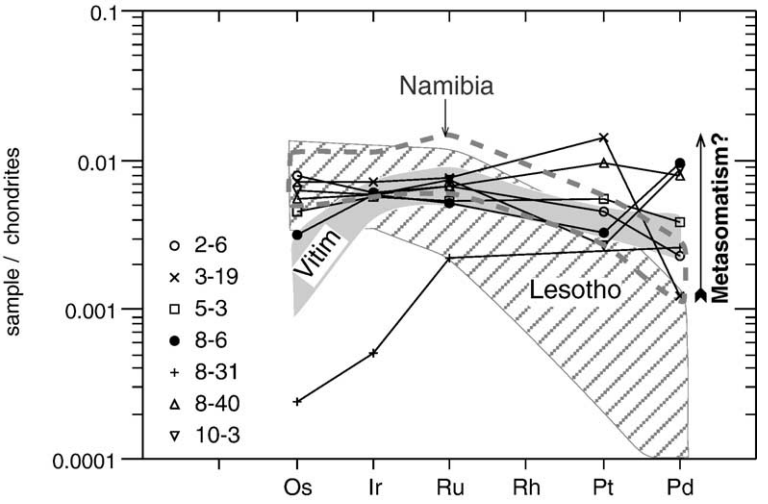

Fig. 6. Chondrite-normalised [37] PGE patterns for Tok peridotites in comparison with those from Vitim, Namibia and Lesotho [12]. The abundances of Os, Ir and Ru in the Tok samples are typically similar, by contrast with the broad range of Pt and Pd. High Pt and Pd in the refractory peridotites are inconsistent with PGE behaviour during partial melting [12] and appear to be due to metasomatic enrichments (indicated by arrow).

and plot in the fields of refractory LH rocks on diagrams of $^{187}Os/^{188}Os$ vs. Os or Al (Figs. 8 and 9). $^{187}Os/^{188}Os$ does not appear to be related to Os abundances (Fig. 9) or to equilibration T° and hence depth (Table 1).

Eight LH series Tok samples plot close to the Al–$^{187}Os/^{188}Os$ trend defined by the Vitim xenolith suite, which yielded systematic correlations of $^{187}Os/^{188}Os$ with partial melting indices [12,16] (Fig. 8a). The same eight Tok xenoliths (as well as 1–2 other samples) define linear correlations of $^{187}Os/^{188}Os$ with other partial melting indices, like MgO or modal cpx (Fig. 8b). All Tok xenoliths that plot above those trends in Fig. 8 have cpx with convex-upward REE–Th–U patterns (Fig. 2) attributed to equilibration with percolating evolved liquids. These xenoliths were classified in Section 3 as strongly metasomatised. By contrast, refractory xenolith 10-17, which yielded lowest $^{187}Os/^{188}Os$ in the Tok suite, has a different, LREE-enriched pattern with lower MREE. As discussed in Section 3, such a pattern likely indicates a lower degree and a different mechanism of metasomatism.

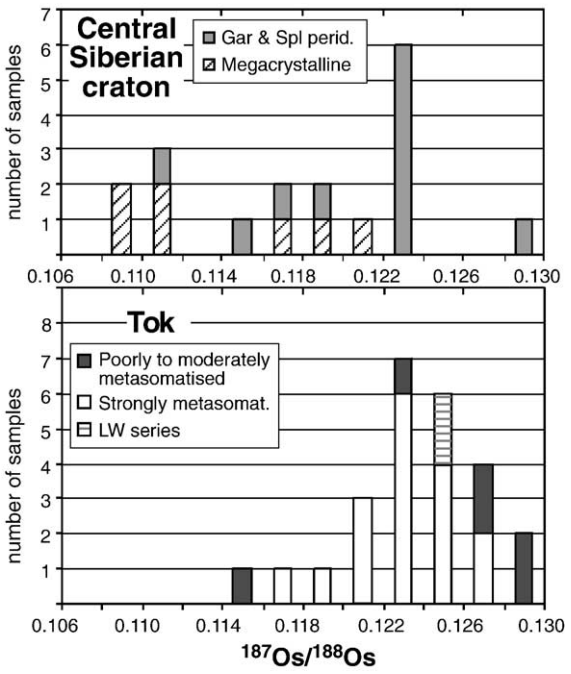

Fig. 7. Frequency distribution of $^{187}Os/^{188}Os$ in peridotite xenoliths from Tok (this study) and in those from Udachnaya and Mir kimberlites [2].

5. Discussion

5.1. Hf–Sr–Nd isotope evidence for depletion and enrichment events

Petrographic and chemical data led Ionov et al. [4–6] to conclude that non-cumulate Tok peridotites originally formed as residues after melt extraction at low depths (≤3 GPa) and that most of those residues later experienced metasomatic alteration ranging from minor chemical and modal effects in fertile LH series peridotites (e.g. enrichments in Na and La) to pervasive metasomatism with large-scale precipitation of cpx and Fe-enrichments (Table 1).

Cpx in the four fertile Tok xenoliths (6-1, 6-2, 8-6, 8-39) have $Sm/Nd_{PM}>1$ (Fig. 2a) and plot in the

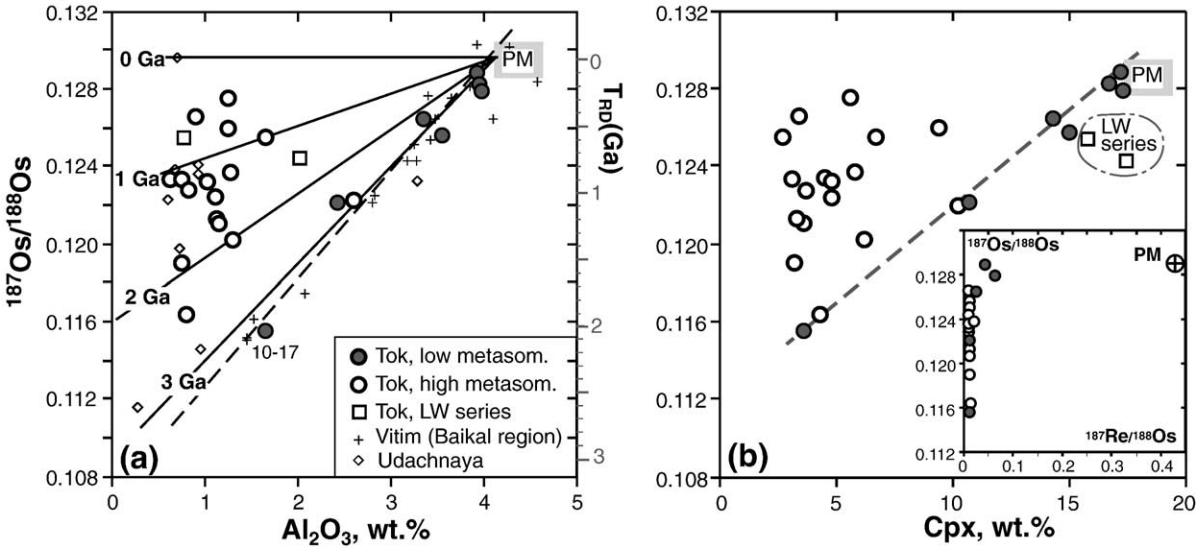

Fig. 8. Variation plots of $^{187}Os/^{188}Os$ vs. Al_2O_3 (a) and modal cpx (b) in Tok xenoliths. Symbols are the same as in Fig. 5. Also shown in (a) are peridotite xenoliths from Vitim [12,16] and Udachnaya [2,70]. T_{RD} ages are calculated relative to present-day bulk Earth (primitive mantle) using $^{187}Os/^{188}Os_{BE}=0.1296$; $^{187}Re/^{188}Os_{BE}=0.4243$; $\lambda^{187}Re=1.666\times10^{-11}$ a^{-1} after [29,71]. The linear correlation for the Vitim xenoliths (dashed line) [12,16] also fits the less metasomatised Tok peridotites. Straight lines in (a) connect PM with model melting residues for 0–3 Ga assuming complete extraction of Al and Re. An inset in (b) shows a plot of $^{187}Re/^{188}Os$ vs. $^{187}Os/^{188}Os$ for the Tok xenoliths.

middle of the MORB field on the Sr–Nd isotope diagram (Fig. 3). These samples may have largely preserved the Nd and Sr isotope signatures of the partial melting event, which initially depleted the peridotites in Rb and in LREE relative to MREE. Their model Nd and Sr isotope ages (relative to BSE) range from 1.2 to 2.8 Ga. These individual dates are very imprecise for a number of reasons. They are model dependant, they are based on Sm and Nd concentrations measured by laser ablation in individual grains while the isotopes were analysed in mineral separates, and metasomatic effects (seen in La–Ce inflections; Fig. 2a) may have affected Nd abundances and isotopic compositions. Yet, taken together, they can be seen as evidence for an ancient (likely Proterozoic) age of the partial melting in the Tok CLM.

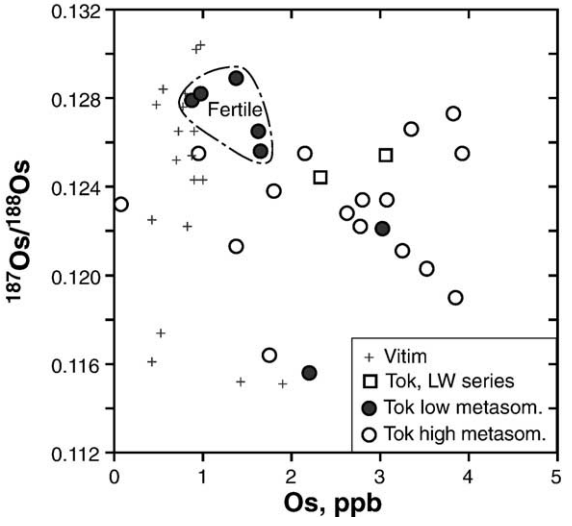

Fig. 9. Plot of $^{187}Os/^{188}Os$ vs. Os abundances in Tok xenoliths. Symbols and sources of other data are the same as in Fig. 5. Note that Os isotopes and abundances are not correlated.

Nd and Sr abundances in other Tok xenoliths (Fig. 2) are too high for partial melting residues [6,16,36]. Sr and Nd isotope compositions in those samples plot in the OIB field and may reflect: (a) different degrees of equilibration of the melting residues with metasomatic fluids, (b) Sr–Nd isotope variations in those fluids and (c) in situ evolution of the Rb–Sr and Sm–Nd systems after the metasomatic event. Importantly, $^{143}Nd/^{144}Nd$ in the strongly metasomatised Tok peridotites and cumulate 8-14 are lower while $^{87}Sr/^{86}Sr$ are higher than in the host basalt (Fig. 3). Thus, even if the metasomatism is a recent event, it cannot have the same source as that of the host magma. Overall, the Sr–Nd isotope correlation for the Tok xenoliths in Fig. 3 can be seen mainly as a result of mixing between the residual mantle and a metasomatic component, which has lower $^{143}Nd/^{144}Nd$ at given $^{87}Sr/^{86}Sr$ than typical Cenozoic alkali basaltic rocks from southern Siberia. Although $^{143}Nd/^{144}Nd$ appears to be positively correlated with $^{147}Sm/^{144}Nd$ in the Tok samples (Fig. 10b), the trend is likely to reflect the complex mixing pro-

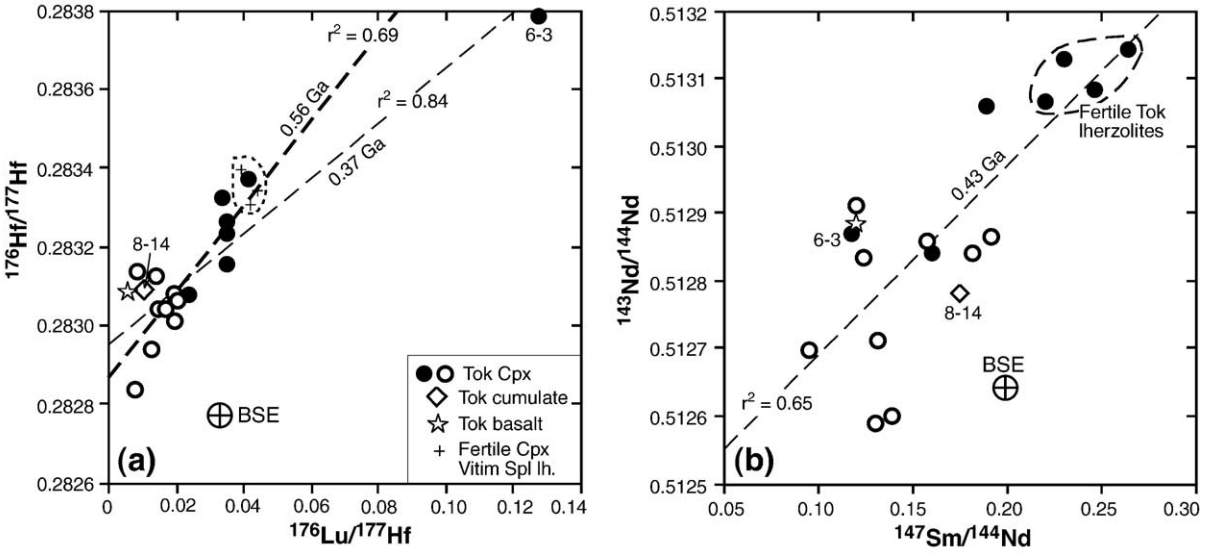

Fig. 10. Plots of $^{176}Lu/^{177}Hf$ vs. $^{176}Hf/^{177}Hf$ (a) and $^{147}Sm/^{144}Nd$ vs. $^{143}Nd/^{144}Nd$ (b) for peridotite xenoliths and host basalt from Tok. BSE, model bulk silicate Earth ([19,72]). Thin dashed lines are linear correlations calculated for all the cpx; thicker grey line in (a) is correlation calculated excluding sample 6-3. Symbols are the same as in Fig. 5.

cesses and has no age meaning. In particular, the high $^{143}Nd/^{144}Nd$ and $^{147}Sm/^{144}Nd$ in the fertile xenoliths are related to partial melting while the lower values in the remainder of the samples are due to later metasomatism as has been seen in xenoliths from the Wyoming craton [28]. Peridotite xenoliths from the Devonian Udachnaya and Mir kimberlites [2,3] show a much broader $^{143}Nd/^{144}Nd$ range than the Tok peridotites consistent with a long-term evolution of the Sm–Nd system in the heterogeneous mantle after ancient fractionation events. This may indicate that the metasomatism in the Tok mantle was a much younger event.

A Lu–Hf isochron plot (Fig. 10a) distinguishes the fertile lherzolites (with high $^{176}Lu/^{177}Hf$ and $^{176}Hf/^{177}Hf$) from the refractory peridotites and cumulate 8-14. Cpx in sample 6-3 (the only one that has a deep negative Hf anomaly relative to HREE, Fig. 2b) has much higher $^{176}Lu/^{177}Hf$ and $^{176}Hf/^{177}Hf$ than all the other Tok cpx. Lu–Hf regressions yield dates of 0.37 Ga for all the cpx and 0.56 Ga excluding 6-3. Similar to the Sm–Nd system, those estimates have no age significance because they reflect a superposition of depletion and enrichments events, which may have taken place at different times. Application of model Lu–Hf ages to the cpx from the Tok peridotites (e.g. ~0.6 Ga for 6-3) cannot be meaningful either because much Lu and Hf in those rocks (much higher proportions than for the Sm–Nd and Rb–Sr systems) reside in the opx (with a distinct Lu/Hf) [17], which was not analysed for Hf isotopic composition.

5.2. The residence and behaviour of PGE

Assuming that PGE abundances in pristine mantle peridotites are close to those in PM (e.g. ~3.4 ppb Os; [34,37]) and taking into account that I-PGE are compatible, residues from high degrees of partial melting of fertile mantle should have higher Os than PM ([1,29], refs. therein). In about half the Tok samples, Os abundances are too low (<2 ppb; Fig. 5) to be consistent with an origin by partial melting of PM, even though they are relatively high compared to many other basalt-hosted xenolith suites, like Vitim (Figs. 5 and 9) ([1], refs. therein). Apparent PGE variations in mantle peridotites are sometimes attributed to the "nugget effect" (heterogeneous distribution of rare, PGE-rich phases) [38]. Such an explanation, however, is not very likely for the low-Os Tok xenoliths because of (1) lack of complementary high-Os analyses (>4 ppb Os), and (2) generally large size of whole-rock samples in this study [4]. Full duplicate analyses of low-Os sample 8-31 at DTM and MPI yielded consistent abundances (~0.1 ppb; Table 3). Random post-eruption loss of PGE due to breakdown of sulfides can also be invoked to explain low Os in basalt-hosted mantle xenoliths [30]. For example, altered interstitial sulfides are common in low-Os, fertile peridotites from Vitim hosted by Miocene tuffs [16]. By contrast, the Tok xenoliths, which occur in young (0.3–0.6 Ma), fresh, massive lavas [4], are practically unaltered and contain few sulfide alteration products.

An important issue in the ongoing debate on the behaviour of PGE in the CLM is the relative role of Fe–Ni–Cu sulfides as their mineral hosts vs. PGE-rich micro-phases, like alloys or I-PGE sulfides [7,31–34,39,40]. Pearson et al. [12] concluded based on a review of experimental and natural data that residual Fe–Ni sulfides are normally exhausted after 20–30% partial melting. Hence, it is likely that I-PGE in at least refractory Tok peridotites reside mainly in the micro-phases, in line with petrographic evidence on the lack of Fe–Ni–Cu sulfides in those rocks (this work; A. Luguet, personal communication, 2005).

By contrast, the scarcity of sulfides in fertile Tok peridotites cannot be attributed to melt extraction because sulfides normally are not fully removed by the low-degrees partial melting that these rocks experienced. The fertile Tok xenoliths also have generally low Os abundances (2–3 times lower than in PM and many refractory peridotites; Fig. 5). Fe–Ni–Cu sulfides may be more prone to breakdown than PGE-rich alloys during or after transport to the surface [12,30], even though such an explanation is not corroborated by petrographic observations on fertile Tok xenoliths. Alternatively, Lorand et al. [41] reported sulfide-poor, non-refractory peridotite xenoliths from the Massif Central, France and argued that metasomatic processes may scavenge sulfides from mantle rocks. In such a case, the consistently low Os in the fertile Tok xenoliths (Fig. 5) may reflect lower stability of Os-bearing Fe–Ni sulfides (presumably present in fertile rocks after the low-degree melting) compared to Os-rich alloys (in refractory rocks) during metasomatism. Although the fertile lherzolites are least metasomatised among the Tok xenoliths, they still may have been affected by sulfide removal, in particular if distinct types of fluids are responsible for mobile behaviour of PGE vs. LREE. By comparison, two LW series wehrlites, which arguably experienced highest degrees of silicate melt percolation among the samples in this study [5], have fairly high Os abundances (2.3–3.0 ppb; Fig. 5). Assuming that I-PGE in those olivine-rich rocks reside in refractory micro-phases rather than Fe–Ni sulfides may explain why they were not affected by metasomatism in the same manner as the lherzolites.

The broad variation in Pt and Pd abundances in the Tok xenoliths is another argument for an important role of metasomatism in the behaviour of PGE in the Tok CLM. Pt and Pd are depleted relative to I-PGE in many residual mantle peridotites worldwide consistent with lower compatibility of Pt and Pd during partial melting ([12], refs. therein). In particular, Pearson et al. [12] reported typically low Pd/Ir_N (0.2 to 0.45) in many on- and off-craton refractory xenolith suites. By contrast, four out of seven Tok xenoliths analysed for PGE have $Pd/Ir_N > 1$ (Table 4). Furthermore, the Pd/Ir_N in the Tok samples are commonly higher than for typically fertile and poorly metasomatised Vitim peridotites (average Pd/Ir_N ~0.65; Fig. 6). We conclude that variably high Pt and Pd in the Tok xenoliths cannot be produced by partial melting or post-eruption alteration and have to be attributed to melt percolation and mantle metasomatism. Such PGE patterns were explained in several earlier studies [41–43] by percolation of late-stage (Pt,Pd)-rich sulfide liquids. The virtual absence of Fe–Ni sulfides in the refractory Tok xenoliths indicates that PGE patterns in mantle peridotites can also be affected by interaction of residual PGE-rich micro-phases with percolating fluids.

5.3. The record of partial melting and metasomatism in Os isotope compositions

A major part of this study is to explain the broad $^{187}Os/^{188}Os$ variation in olivine-rich Tok peridotites (Figs. 8 and 9). The Re–Os system has generally shown itself to be a reliable means for model age dating of melting events in the mantle because Re is almost completely removed by melting, thus preserving ancient Os isotopic compositions [44]. Also the high Os contents of xenoliths make them impervious to contamination by host magmas or trapped metasomatic melts [1,29,45,46]. Many recent studies, however, furnished evidence that the Re–Os system in mantle peridotites can be variably affected by late-stage melt percolation and metasomatism [9,13,28,32,47–50]. Sr–Nd–Hf isotope data in this study, together with petrographic and chemical data [4–6], show that especially the refractory Tok peridotites have experienced pervasive metasomatism. This comprehensive chemical and isotope data set enables the possible effects of the metasomatism on the Re–Os system in the Tok mantle to be distinguished from the time-integrated record of earlier partial melting events which, surprisingly, are better preserved in the more fertile spinel lherzolites.

$^{187}Re/^{188}Os$ in the Tok xenoliths do not show regular correlations with $^{187}Os/^{188}Os$ (Fig. 8b inset) and therefore typical parent–daughter decay cannot be used for age estimates. As discussed above, the most likely reason for that is variable removal of Re and Os after the partial melting. It may be possible, however, to obtain age information by exploring links between Os isotope compositions and robust partial melting indices, like Al_2O_3 contents [51–54]. We assume that Re and Os abundances in the Tok peridotites were initially estab-

lished by residue/melt partitioning and if any loss of Re and Os took place, it happened relatively recently. We also assume that residue/melt partitioning is similar for Re and Al and use whole-rock Al_2O_3 contents vs. $^{187}Os/^{188}Os$ to assess relative time-integrated Re/Os values in the samples. In such a model, samples with the same age should plot on an Al_2O_3–$^{187}Os/^{188}Os$ plot along a line connecting PM with a point, at which Re/Os becomes close to zero. Such lines are shown in Fig. 8a assuming that Re/Os ~0 at Al ~0 [52]. Some authors [51,53] argued that this approach overestimates ages because some Al is left behind in high-T opx in harzburgitic residues after all Re is exhausted. This is probably correct but not directly relevant to our discussion, which focuses on relative ages.

Fertile and poorly metasomatised refractory Tok xenoliths plot in Fig. 8a around a 2.8 Ga line suggesting that this suite may record the oldest melting-related event. Slightly older ~3 Ga ages are typically seen in xenolith suites from the interior of the Siberian craton [2,53]. The remainder of the Tok samples is scattered between lines corresponding to ages from recent to >2 Ga, which could imply that the Tok CLM has experienced multiple melting events since early Proterozoic. This is unlikely for several reasons. First, intermediate compositions ($1.6<Al_2O_3<3.5\%$) are lacking except for the samples recording the Al_2O_3–$^{187}Os/^{188}Os$ of the oldest event, which thus is the only one with a progressive change of composition with melting. Second, high degrees of melting (>20%; [4]) are required to yield the refractory Tok peridotites, which is only possible in large-scale tectono-thermal events (e.g. arrival of a mantle plume, protracted subduction and lithospheric thickening). Such events may be the cause of the initial lithospheric formation but are less likely to affect the same rocks repeatedly once they had become a refractory portion of the lithospheric mantle.

It appears that melting alone cannot produce the observed $^{187}Os/^{188}Os$ range in the refractory Tok xenoliths (we also note that many low-Al Udachnaya peridotites have elevated $^{187}Os/^{188}Os$ similar to the Tok xenoliths; Fig. 8a). The most likely alternative is to attribute the $^{187}Os/^{188}Os$ variations to relatively recent metasomatism. In such a model, the Tok CLM was produced by an ancient large-scale melting event and the highly refractory peridotites initially plotted in Fig. 8a close to the low-Al extreme of the 3 Ga evolution line defined by the fertile and moderately refractory samples. $^{187}Os/^{188}Os$ in the refractory peridotites were then variably affected by the recent metasomatic event to yield a range of $^{187}Os/^{188}Os$ shifted towards that of the metasomatic melt/fluid. Importantly, some of the highest $^{187}Os/^{188}Os$ are shown by two wehrlites, which experienced highest degrees of silicate melt percolation [5]. None of the metasomatised Tok xenoliths has $^{187}Os/^{188}Os$ higher than in PM, which indicates that the melt probably came from an asthenospheric mantle source and does not contain highly radiogenic components of crustal origin (e.g. subduction-related [8,10,11]). Such crustal sources would also have high Re contents and would likely have raised the Re content of the peridotite, which is not seen. The refractory peridotites (but not the fertile ones) were selectively affected by the metasomatism because of wetting behaviour of the peridotite-melt system, which is controlled by olivine/pyroxene ratios [55–57] such that olivine-rich rocks are highly permeable while fertile, pyroxene-rich rocks are less so.

Common high Pd/Ir and Pt/Ir in the refractory Tok xenoliths (Table 4; Fig. 6) is an important piece of evidence that the metasomatism affected not only lithophile elements (Figs. 2 and 11) but also PGE. The broad range of both PGE patterns (Fig. 6) and $^{187}Os/^{188}Os$ (Fig. 8) in the metasomatised peridotites may indicate a variety of processes and fluid compositions. It is not likely however that PGE-rich phases, either sulfides or alloys, were mechanically transported by the melt because that could locally produce very high PGE abundances, which are not seen in the Tok xenoliths (all have Os<4 ppb). Ionov et al. [4,6] identified at least two series of metasomatic events: (1) large-scale percolation of evolved silicate melts followed by (2) infiltration of small-volume melts rich in alkalis, phosphorus and volatiles. It is not clear, which of them affected PGE more. On one hand, high melt/rock ratios may be required to affect $^{187}Os/^{188}Os$ in the peridotites because Os abundances in silicate melts are much lower than in peridotites [13,49,50]. On the other hand, PGE may be particularly mobile in alkali-rich small-volume melts because of chemical complexing [47,58,59].

The latter hypothesis seems to be supported by the fact that all four phosphate-rich ($P_2O_5 \geq 0.08\%$; [4,6]) Tok xenoliths in this study yield fairly high (relative to their presumed ancient protoliths) $^{187}Os/^{188}Os>0.122$. However, $^{187}Os/^{188}Os$ or Pd/Ir in the olivine-rich Tok xenoliths on the whole do not show regular correlations with the contents of P_2O_5, alkalis or LREE. While variable enrichments in alkalis and LREE are common in many refractory peridotite series worldwide, a particular feature of olivine-rich Tok peridotites is elevated abundances of more compatible lithophile elements, like HREE, which are commonly considered as robust partial melting indices poorly affected by metasoma-

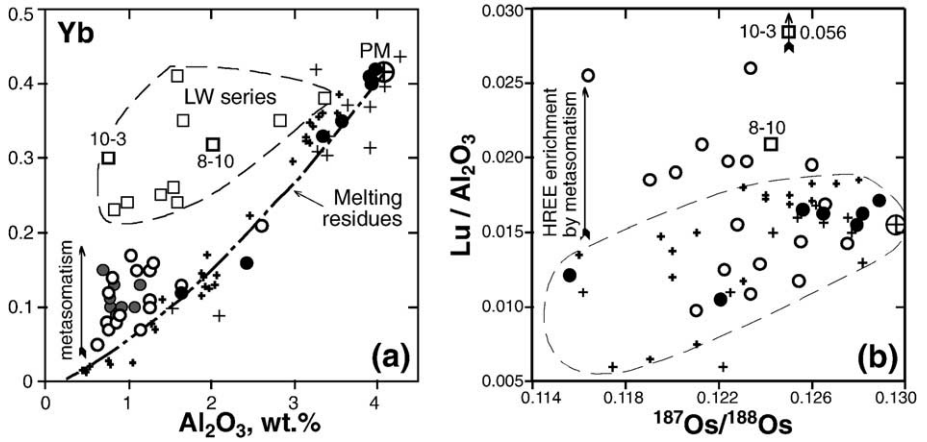

Fig. 11. Plots of Yb (in ppm) vs. Al_2O_3 (wt.%) (a) and Lu/Al_2O_3 vs. $^{187}Os/^{188}Os$ (b) in xenoliths from Tok (Al, Lu and Yb contents are from [4–6]) and Vitim. Symbols and other data sources are the same as in Fig. 5. Also shown (small grey crosses) are peridotites from the Horoman massif [60,73]. Note that HREE abundances and Lu/Al_2O_3 in many olivine-rich Tok peridotites must have been increased by metasomatism because they are higher than in residues after melt extraction from fertile spinel peridotites.

tism (e.g. [1,51]). Fig. 11 shows that Yb abundances at given Al_2O_3 in the majority of olivine-rich Tok xenoliths are higher than in poorly metasomatised peridotites from the Horoman massif and Vitim or estimates for partial melting residues [6,60] and that many Tok peridotites have unusually high Lu/Al. However, the metasomatic enrichments in middle to heavy REE do not appear to be correlated with elevated Pd/Ir or $^{187}Os/^{188}Os$ in individual samples (Fig. 11b). It appears that metasomatism of refractory peridotites by percolating melts at high time-integrated melt/rock ratios creates favourable conditions for the enrichments in Pt and Pd and radiogenic Os but whether such enrichments indeed take place as speculated above depends on additional factors or processes, which we are as yet unknown.

As noted above, effects of metasomatism on Os isotope compositions have been invoked for several other peridotite suites. Although we call for essentially the same processes in this study, our data and inferences for the Tok suite show some significant differences with earlier work. Most importantly, the scope of inferred enrichments in radiogenic $^{187}Os/^{188}Os$ is greater and the proportion of the enriched xenoliths in their total population is higher than in previous studies. For example, minor enrichments in radiogenic Os were inferred for only a small proportion of studied xenoliths from Somerset Island [32] and only for those rare xenoliths from Tanzania [48] that contain pockets and veins of metasomatic minerals and glass. Also, the range of $^{187}Os/^{188}Os$ reported for pervasively metasomatised harzburgites from the Kenya rift [13] is relatively narrow (0.112–0.118) compared to that in Tok harzburgites (0.116 to 0.128). As discussed above, we attribute the latter range to variable increases in $^{187}Os/^{188}Os$ from ≤0.115 up to 0.128 to be caused by metasomatism.

Altogether, the widespread, large-scale enrichments in radiogenic $^{187}Os/^{188}Os$ in the Tok suite have effectively erased the evidence for ancient melt extraction in the highly refractory peridotites thus rendering the Re–Os data on those rocks unsuitable for dating. Hence, if our model is correct, this study shows that metasomatic effects on the Re–Os system in some portions of the CLM may be much more dramatic than previously thought (e.g. [13,45]). In particular, pervasive percolation metasomatism at high time-integrated melt/rock ratios may perturb and even re-set the Re–Os system in large ancient mantle domains as it did at Tok. Important indicators of such metasomatism are enrichments in MREE–HREE and convex-upward REE patterns of cpx (Fig. 2c), i.e. evidence for high degrees of equilibration with percolating silicate melts. The combined chemical and isotope data on the Tok xenolith suite show that these features are better indicators of this type of perturbation of the Re–Os system (leading to elevated $^{187}Os/^{188}Os$) than other commonly used indices of metasomatism such as strong enrichments in LREE (Fig. 2a) or precipitation of accessory amphibole or phlogopite. The latter features are rather indicative of a different type of metasomatism (entrapment of small-volume, volatile-rich melts) or early stages of melt percolation (low melt/rock) [5], which are less likely to affect the Re–Os system (e.g. [61]).

We further speculate that the broad scatter of $^{187}Os/^{188}Os$ and their poor correlation with partial

melting indices reported for some other peridotite suites, e.g. xenoliths from Louwrencia kimberlite in Namibia [12] or some ophiolites [62], may have been caused (or at least enhanced) by the same process. In such a case, looking through the veil of metasomatism may require the analysis of large numbers of samples focusing on less strongly metasomatised, moderately refractory peridotites.

Refractory CLM from the interiors of cratons appears to have been generally immune from such large-scale metasomatic effects on $^{187}Os/^{188}Os$ [44,53,63,64]. This is probably because such processes require high melt/rock ratios, large quantities of melt, and immense heat sources, which can rarely match the great thickness and low temperatures of cratonic CLM with deep keels. Upwelling of asthenosperic material is commonly stopped at great depths (>200 km) under the cratonic keels and is unlikely to produce large quantities of basaltic magma by decompression melting, but instead yields small-fraction kimberlite and carbonatite liquids. Thus, the lower cratonic lithosphere can effectively shield the central and upper CLM sections from metasomatism that requires high melt/rock ratios such that thick, rigid and cold inner parts of cratonic CLM are basically impenetrable for large-scale percolation of high-T basaltic magmas. Geochemical studies of cratonic xenoliths show that they are mainly metasomatised by trapped low-T, volatile-rich liquids similar to kimberlites (e.g. [1,65]). In situ dating of sulfides in Kaapvaal xenoliths [66] shows that sulfide T_{RD} model ages tend to decrease with Fe-(+/−Al, Ca) metasomatism, attributed to asthenosphere-derived silicate melts, and that such metasomatism is most prominent toward the base of the lithospheric mantle. Hence, $^{187}Os/^{188}Os$ in the shallow CLM can be elevated by metasomatism on a large-scale only at craton margins (e.g. Aldan schield, Namibia), in rifted areas and in off-craton domains with generally thin CLM.

5.4. The age of the CLM beneath Tok and the structure of the Siberian craton

Sample 10-17 with lowest $^{187}Os/^{188}Os$ yields rhenium depletion age of ~2 Ga. This value is identical to the age of a regional mid-Proterozoic (1.9–2.0 Ga) metamorphic event, which amalgamated older terrains in the Stanovoy block and was accompanied by widespread magmatism ([4], refs. therein). The ages obtained for individual granite-greenstone and granulite-gneiss terrains on the Aldan schield in the vicinity of Tok range from 1.9 to 3.6 Ga.

We further note that xenolith 10-17 has higher Al_2O_3 (1.6%) than most other refractory peridotites in this study. Hence, we cannot rule out that the more olivine-rich Tok peridotites had even lower $^{187}Os/^{188}Os$ before the inferred metasomatic event based on Al–$^{187}Os/^{188}Os$ trends common in less metasomatised peridotite series [12,13,51,52,54]. Projection of those samples onto the Al–Os correlation (Fig. 8a) defined by the less refractory peridotites yields model ages (T_{RD}) from 2 to 2.8 Ga. These rough estimates are younger than the oldest dates reported for xenoliths from the central Siberian craton [2], but older than those recently obtained for off-craton xenoliths from southern Siberia [12,16] and Mongolia [67]. As recently discussed by Ionov et al. [4], there are no reasons to assume tectonic contiguity or simultaneous formation for the whole Siberian craton. Younger formation ages for the SE margin of the craton could be consistent with successive accretion of younger terrains around the ancient craton core with a deep keel.

The pervasive metasomatic alteration and the likely absence of the deep keel in the Tok CLM [4] may be consistent with its position on the craton margin, which was in the direct vicinity of the subduction system in the NW Pacific in the late Mesozoic to early Cenozoic. Mafic magmatism and the formation of large, coal-bearing grabens at that time [68] indicate that those events profoundly affected the lithosphere in the Tok area and could have triggered the destruction of the cratonic keel (if it ever existed) and/or a series of metasomatic events. The last of them may be related to the late Cenozoic basaltic volcanism.

6. Summary

This study provides the first constraints on the age of the lithospheric mantle in the SE Siberian craton as well as further insights into the effects of pervasive mantle metasomatism on the CLM. Altogether, the new radiogenic isotope results and available chemical data on the Tok xenoliths indicate large-scale metasomatic re-working of their original residual 'protoliths'. The age of melt depletion is best expressed in the least metasomatised spinel peridotites which show Al_2O_3 and modal cpx vs. $^{187}Os/^{188}Os$ correlations giving model ages of 2.0 to 2.8 Ga. In strongly metasomatised olivine-rich peridotites, the metasomatic transformation effectively erases both trace element and time-integrated radiogenic isotope evidence for the ancient melting events (that are commonly present in refractory peridotites elsewhere) and imparts geochemical signatures of enriched fluids. In particular, Hf, Nd, Sr and Os isotope compositions and

PGE patterns have been profoundly affected by the metasomatism. Hf, Nd and Sr isotopic compositions of the xenoliths overlap the fields for oceanic basalts, and in some cases $^{187}Os/^{188}Os$ have been raised to that of the present depleted asthenospheric mantle. The trace element effects of the metasomatic process are evident in REE enrichments that produce convex-upward REE patterns as well as clear Pd and Pt enrichments on PGE patterns. Work on these same Tok xenoliths presented earlier [4–6] identified at least two series of metasomatic events: large-scale percolation of evolved silicate melts followed by infiltration of small-volume melts rich in alkalis, phosphorus and volatiles. It is not known which of these two metasomatic agents has a greater effect on the PGE and Os. The radiogenic isotope compositions in the strongly metasomatised xenoliths suggest this process occurred in late Phanerozoic. It is therefore a much younger overprint on the earlier Archean to Proterozoic melt extraction, which could be related to subduction in the NW Pacific at this time. These results characterize the uppermost mantle beneath the SE Siberian craton as one of the most strongly metasomatised CLM domains worldwide and provide a glimpse of the detailed effects of such metasomatism.

Acknowledgements

DAI thanks V. Prikhodko (ITIG, Far Eastern Branch, Russian Academy of Sciences) for help with fieldwork in Siberia; support by Al Hofmann at Mainz and G. Brey in Frankfurt is greatly appreciated. Analytical and other assistance was provided by M. Horan, R. Carlson, N. Mattielli, J. Lassiter, K. Zentel. Funding for analytical work at ULB was from FNRS Grant #4.4607.01 to DW. Funding for DAI in Germany was provided by A. von Humboldt Foundation (Wiederaufname fellowship), DFG (Mercator guest professorship) and MPG. We appreciate reviews by T. Meisel and anonymous reviewer and editorial comments by K. Farley.

Appendix A. Supplementary data

Supplementary data associated with this article can be found, in the online version, at doi:10.1016/j.epsl.2005.10.038.

References

[1] D.G. Pearson, D. Canil, S.B. Shirey, Mantle samples included in volcanic rocks: xenoliths and diamonds, in: R.W. Carlson (Ed.), Treatise on Geochemistry, vol. 2. The Mantle and Core, Elsevier, 2003, pp. 171–276.

[2] D.G. Pearson, S.B. Shirey, R.W. Carlson, F.R. Boyd, N.P. Pokhilenko, N. Shimizu, Re–Os, Sm–Nd, and Rb–Sr isotope evidence for thick Archaean lithospheric mantle beneath the Siberian craton modified by multistage metasomatism, Geochim. Cosmochim. Acta 59 (1995) 959–977.

[3] A.Z. Zhuravlev, Y.Y. Laz'ko, A.I. Ponomarenko, Radiogenic isotopes and REE in garnet peridotite xenoliths from the Mir kimberlite pipe, Yakutia, Geochem. Int. (1992) 45–56.

[4] D.A. Ionov, V.S. Prikhodko, J.-L. Bodinier, A.V. Sobolev, D. Weis, Lithospheric mantle beneath the south-eastern Siberian craton: petrology of peridotite xenoliths in basalts from the Tokinsky Stanovik, Contrib. Mineral. Petrol. 149 (2005) 647–665.

[5] D.A. Ionov, I. Chanefo, J.-L. Bodinier, Origin of Fe-rich lherzolites and wehrlites from Tok, SE Siberia by reactive melt percolation in refractory mantle peridotites, Contrib. Mineral. Petrol. 150 (2005) 335–353.

[6] D.A. Ionov, G. Chazot, C. Chauvel, C. Merlet, J.-L. Bodinier. Trace element distribution in peridotite xenoliths from Tok, SE Siberian craton: evidence for pervasive, multi-stage metasomatism in shallow refractory mantle, Geochim. Cosmochim. Acta (in press).

[7] O. Alard, W.L. Griffin, J.-P. Lorand, S.E. Jackson, S.Y. O'Reilly, Non-chondritic distribution of the highly siderophile elements in mantle sulfides, Nature 407 (2000) 891–894.

[8] A. Büchl, G. Brügmann, V.G. Batanova, C. Munker, A.W. Hofmann, Melt percolation monitored by Os isotopes and HSE abundances: a case study from the mantle section of the Troodos Ophiolite, Earth Planet. Sci. Lett. 204 (2002) 385–402.

[9] G. Schmidt, J. Snow, Os isotopes in mantle xenoliths from the Eifel volcanic field and the Vogelsberg (Germany): age constraints on the lithospheric mantle, Contrib. Mineral. Petrol. 143 (2002) 694–705.

[10] E. Widom, P. Kepezhinskas, M.J. Defant, The nature of metasomatism in the sub-arc mantle wedge: evidence from Re–Os isotopes in Kamchatka peridotite xenoliths, Chem. Geol. 196 (2003) 283–306.

[11] J. Chesley, K. Righter, J. Ruiz, Large-scale mantle metasomatism: a Re–Os perspective, Earth Planet. Sci. Lett. 219 (2004) 49–60.

[12] D.G. Pearson, G.J. Irvine, D.A. Ionov, F.R. Boyd, G.E. Dreibus, Re–Os isotope systematics and platinum group element fractionation during mantle melt extraction: a study of massif and xenolith peridotite suites, Chem. Geol. 208 (2004) 29–59.

[13] L. Reisberg, J.-P. Lorand, R.M. Bedini, Reliability of Os model ages in pervasively metasomatized continental mantle lithosphere: a case study of Sidamo spinel peridotite xenoliths (East African Rift, Ethiopia), Chem. Geol. 208 (2004) 119–140.

[14] D.A. Ionov, J.-L. Bodinier, S.B. Mukasa, A. Zanetti, Mechanisms and sources of mantle metasomatism: major and trace element compositions of peridotite xenoliths from Spitsbergen in the context of numerical modeling, J. Petrol. 43 (2002) 2219–2259.

[15] J.-L. Bodinier, M.A. Menzies, N. Shimizu, F.A. Frey, E. McPherson, Silicate, hydrous and carbonate metasomatism at Lherz, France: contemporaneous derivatives of silicate melt-harzburgite reaction, J. Petrol. 45 (2004) 299–320.

[16] D.A. Ionov, I. Ashchepkov, E. Jagoutz, The provenance of fertile off-craton lithospheric mantle: Sr–Nd isotope and chemical composition of garnet and spinel peridotite xenoliths from Vitim, Siberia, Chem. Geol. 217 (2005) 41–75.

[17] D.A. Ionov, J. Blichert-Toft, D. Weis, Hf isotope compositions and HREE variations in off-craton garnet and spinel peridotite xenoliths from central Asia, Geochim. Cosmochim. Acta 69 (2005) 2399–2418.
[18] S.V. Rasskazov, A. Boven, A.V. Ivanov, V.G. Semenova, Middle quaternary volcanic impulse in the Olekma–Stanovoy mobile system: ^{40}Ar–^{39}Ar dating of volcanics from the Tokinsky Stanovik, in: Tikhookeanskaya Geologiya, vol. 19, 2000, pp. 19–28 (in Russian).
[19] A. Zindler, S. Hart, Chemical geodynamics, Annu. Rev. Earth Planet. Sci. 14 (1986) 493–571.
[20] A.W. Hofmann, Mantle geochemistry: the message from oceanic volcanism, Nature 385 (1997) 219–229.
[21] D.A. Ionov, S.Y. O'Reilly, I.V. Ashchepkov, Feldspar-bearing lherzolite xenoliths in alkali basalts from Hamar-Daban, southern Baikal region, Russia, Contrib. Mineral. Petrol. 122 (1995) 174–190.
[22] J.S. Johnson, S.A. Gibson, R.N. Thompson, G.M. Nowell, Volcanism in the vitim volcanic field, Siberia: geochemical evidence for a mantle plume beneath the Baikal Rift Zone, J. Petrol. 46 (2005) 1309–1344.
[23] Y. Nishio, S. Nakai, J. Yamamoto, H. Sumino, T. Matsumoto, V.S. Prikhod'ko, S. Arai, Lithium isotopic systematics of the mantle-derived ultramafic xenoliths: implications for EM1 origin, Earth Planet. Sci. Lett. 217 (2004) 245–261.
[24] V. Malkovets, D. Ionov, A. Agashev, Y. Litasov, Y. Orihashi, S. O'Reilly, W. Griffin, Structure and composition of the mantle beneath the Minusa region of the Siberian craton: a Sr–Nd isotope and trace element study, J. Conf. Abstr. 5/2 (2000) (abstr. #662).
[25] A.W. Hofmann, Sampling mantle heterogeneity through oceanic basalts: isotopes and trace elements, in: R.W. Carlson (Ed.), Treatise on Geochemistry, vol. 2. The Mantle and Core, Elsevier, 2003, pp. 61–102.
[26] S.S. Schmidberger, A. Simonetti, D. Francis, C. Gariepy, Probing Archean lithosphere using the Lu–Hf isotope systematics of peridotite xenoliths from Somerset Island kimberlites, Canada, Earth Planet. Sci. Lett. 197 (2002) 245–259.
[27] M. Bizimis, G. Sen, V.J.M. Salters, Hf–Nd isotope decoupling in the oceanic lithosphere: constraints from spinel peridotites from Oahu, Hawaii, Earth Planet. Sci. Lett. 217 (2004) 43–58.
[28] R.W. Carlson, A.J. Irving, D.J. Schulze, B.C. Hearn Jr., Timing of Precambrian melt depletion and Phanerozoic refertilization events in the lithospheric mantle of the Wyoming Craton and adjacent Central Plains Orogen, Lithos 77 (2004) 453–472.
[29] S.B. Shirey, R.J. Walker, The Re–Os isotope system in cosmochemistry and high-temperature geochemistry, Annu. Rev. Earth Planet. Sci. 26 (1998) 423–500.
[30] M.R. Handler, V.C. Bennett, G. Dreibus, Evidence from correlated Ir/Os and Cu/S for late-stage Os mobility in peridotite xenoliths: implications for Re–Os systematics, Geology 27 (1999) 75–78.
[31] C.-T.A. Lee, Platinum-group element geochemistry of peridotite xenoliths from the Sierra Nevada and the Basin and Range, California, Geochim. Cosmochim. Acta 66 (2002) 3987–4005.
[32] G.J. Irvine, D.G. Pearson, B.A. Kjarsgaard, R.W. Carlson, M.G. Kopylova, G. Dreibus, A Re–Os isotope and PGE study of kimberlite-derived peridotite xenoliths from Somerset Island and a comparison to the Slave and Kaapvaal cratons, Lithos 71 (2003) 461–488.
[33] R.H. Mitchell, R.R. Keays, Abundance and distribution of Au, Pd and Ir in some spinel and garnet lherzolites: implications for the nature and origin of precious metal-rich intergranular components in the upper mantle, Geochim. Cosmochim. Acta 45 (1981) 2425–2442.
[34] J.W. Morgan, Ultramafic xenoliths: clues to Earth's late accretional history, J. Geophys. Res. 91 (1986) 12375–12387.
[35] J.P. Lorand, M. Gros, L. Pattou, Fractionation of platinum-group elements in the upper mantle: a detailed study in Pyrenean orogenic peridotites, J. Petrol. 40 (1999) 951–987.
[36] E. Hellebrand, J.E. Snow, H.J.B. Dick, A.W. Hofmann, Coupled major and trace elements as indicators of the extent of melting in mid-ocean-ridge peridotites, Nature 410 (2001) 677–681.
[37] W.F. McDonough, S.-s. Sun, The composition of the Earth, Chem. Geol. 120 (1995) 223–253.
[38] M. Rehkämper, A.N. Halliday, D. Barford, J.G. Fitton, J.B. Dawson, Platinum-group element abundance patterns in different mantle environments, Science 278 (1997) 1595–1598.
[39] J.-P. Lorand, L. Reisberg, R.M. Bedini, Platinum-group elements and melt percolation processes in Sidamo spinel peridotite xenoliths, Ethiopia, East African Rift, Chem. Geol. 196 (2003) 57–75.
[40] A. Luguet, J.-P. Lorand, O. Alard, J.-Y. Cottin, A multi-technique study of platinum group element systematic in some Ligurian ophiolitic peridotites, Italy, Chem. Geol. 208 (2004) 175–194.
[41] J.-P. Lorand, O. Alard, A. Luguet, R.R. Keays, Sulfur and selenium systematics of the subcontinental lithospheric mantle: inferences from the Massif Central xenolith suite (France), Geochim. Cosmochim. Acta 67 (2003) 4137–4151.
[42] M. Rehkämper, A.N. Halliday, J. Alt, J.G. Fitton, J. Zipfel, E. Takazawa, Non-chondritic platinum-group element ratios in oceanic mantle lithosphere: petrogenetic signature of melt percolation?, Earth Planet. Sci. Lett. 172 (1999) 65–81.
[43] A. Luguet, J.-P. Lorand, M. Seyler, Sulfide petrology and highly siderophile element geochemistry of abyssal peridotites: a coupled study of samples from the Kane Fracture Zone (45°W 23°20N, MARK area, Atlantic Ocean), Geochim. Cosmochim. Acta 67 (2003) 1553–1570.
[44] R.J. Walker, R.W. Carlson, S.B. Shirey, F.R. Boyd, Os, Sr, Nd, and Pb isotope systematics of southern African peridotite xenoliths: Implications for the chemical evolution of subcontinental mantle, Geochim. Cosmochim. Acta 53 (1989) 1583–1595.
[45] M.R. Handler, V.C. Bennett, T.M. Esat, The persistence of off-cratonic lithospheric mantle: Os isotopic systematics of variably metasomatised southeast Australian xenoliths, Earth Planet. Sci. Lett. 151 (1997) 61–75.
[46] V. Olive, R.M. Ellam, B. Harte, A Re–Os isotope study of ultramafic xenoliths from the Matsoku kimberlite, Earth Planet. Sci. Lett. 150 (1997) 129–140.
[47] A.D. Brandon, R.A. Creaser, S.B. Shirey, R.W. Carlson, Osmium recycling in subduction zones, Science 272 (1996) 861–864.
[48] J.T. Chesley, R.L. Rudnick, C.-T. Lee, Re–Os systematics of mantle xenoliths from the East African Rift: age structure, and history of the Tanzanian craton, Geochim. Cosmochim. Acta 63 (1999) 1203–1217.
[49] H. Becker, S.B. Shirey, R.W. Carlson, Effects of melt percolation on the Re–Os systematics of peridotites from a Paleozoic convergent plate margin, Earth Planet. Sci. Lett. 188 (2001) 107–121.
[50] A. Büchl, G.E. Brügmann, V.G. Batanova, A.W. Hofmann, Os mobilization during melt percolation: the evolution of Os isotope heterogeneities in the mantle sequence of the Troodos

ophiolite, Cyprus, Geochim. Cosmochim. Acta 68 (2004) 3397–3408.
[51] O.M. Burnham, N.W. Rogers, D.G. Pearson, P.W. van Calsteren, C.J. Hawkesworth, The petrogenesis of the eastern Pyrenean peridotes: an integrated study of their whole-rock geochemistry and Re–Os isotope composition, Geochim. Cosmochim. Acta 62 (1998) 2293–2310.
[52] L. Reisberg, J.P. Lorand, Longevity of sub-continental mantle lithosphere from osmium isotope systematics in orogenic peridotite massifs, Nature 376 (1995) 159–162.
[53] D.G. Pearson, The age of continental roots, Lithos 48 (1999) 171–194.
[54] A.H. Peslier, L. Reisberg, J. Ludden, D. Francis, Os isotopic systematics in mantle xenoliths: age constraints on the Canadian Cordillera lithosphere, Chem. Geol. 166 (2000) 85–101.
[55] A. Toramaru, N. Fujii, Connectivity of melt phase in a partially molten peridotite, J. Geophys. Res. 91 (1986) 9239–9252.
[56] U.H. Faul, Permeability of partially molten upper mantle rocks from experiments and percolation theory, J. Geophys. Res. 102 (1997) 10299–10311.
[57] M.J. Daines, Melt distribution in partially molten peridotite: implications for permeability and melt migration in the upper mantle, in: M.B. Holness (Ed.), Deformation-enhanced Fluid Transport in the Earth's Crust and Mantle, Chapman and Hall, London, 1997, pp. 62–81.
[58] J.-P. Lorand, O. Alard, Platinum-group element abundances in the upper mantle: new constraints from in situ and whole-rock analyses of Massif Central xenoliths (France), Geochim. Cosmochim. Acta 65 (2001) 2789–2806.
[59] J.-P. Lorand, G. Delpech, M. Gregoire, B. Moine, S.Y. O'Reilly, J.-Y. Cottin, Platinum-group elements and the multistage metasomatic history of Kerguelen lithospheric mantle (South Indian Ocean), Chem. Geol. 208 (2004) 195–215.
[60] E. Takazawa, F.A. Frey, N. Shimizu, M. Obata, Whole rock compositional variations in an upper mantle peridotite (Horoman, Hokkaido, Japan): are they consistent with a partial melting process, Geochim. Cosmochim. Acta 64 (2000) 695–716.
[61] L. Reisberg, X. Zhi, J.-P. Lorand, C. Wagner, Z. Peng, C. Zimmermann, Re–Os and S systematics of spinel peridotite xenoliths from east central China: evidence for contrasting effects of melt percolation, Earth Planet. Sci. Lett. 239 (2005) 286–308.
[62] J.E. Snow, G. Schmidt, E. Rampone, Os isotopes and highly siderophile elements (HSE) in the Ligurian ophiolites, Italy, Earth Planet. Sci. Lett. 175 (2000) 119–132.
[63] D.G. Pearson, R.W. Carlson, S.B. Shirey, F.R. Boyd, P.H. Nixon, Stabilisation of Archaen lithospheric mantle: a Re–Os isotope study of peridotite xenoliths from the Kaapvaal craton, Earth Planet. Sci. Lett. 134 (1995) 341–357.
[64] R.W. Carlson, D.G. Pearson, F.R. Boyd, S.B. Shirey, G. Irvine, A.H. Menzies, J.J. Gurney, Re–Os systematics of lithosphere peridotites: implications for lithosphere formation and preservation, in: J.J. Gurney, J.L. Gurney, M.D. Pascoe, S.H. Richardson (Eds.), Proc. 7th Internatl. Kimberlite Conf. 1, RedRoof Design, Cape Town, 1999, pp. 99–108.
[65] M. Grégoire, D.R. Bell, A.P. Le Roex, Garnet lherzolites from the Kaapvaal Craton (South Africa): trace element evidence for a metasomatic history, J. Petrol. 44 (2003) 629–657.
[66] W.L. Griffin, S. Graham, S.Y. O'Reilly, N.J. Pearson, Lithosphere evolution beneath the Kaapvaal Craton: Re–Os systematics of sulfides in mantle-derived peridotites, Chem. Geol. 208 (2004) 89–118.
[67] D.A. Ionov, J.C. Lassiter, A.W. Hofmann, The age of the lithospheric mantle in the Central Asian Orogenic Belt from Os isotope data on xenoliths, Geochim. Cosmochim. Acta 68 (2004) A712 (abstr.).
[68] L.P. Zonenshain, M.I. Kuzmin, L.M. Natapov, Geology of the USSR: A Plate Tectonic Synthesis, Amer. Geophys. Union, Geodynamics Ser. 21, Washington, D.C., 1990, 242 pp.
[69] A.W. Hofmann, Chemical differentiation of the Earth: the relationship between mantle, continental crust, and oceanic crust, Earth Planet. Sci. Lett. 90 (1988) 297–314.
[70] F.R. Boyd, N.P. Pokhilenko, D.G. Pearson, S.A. Mertzman, N.V. Sobolev, L.W. Finger, Composition of the Siberian cratonic mantle: evidence from Udachnaya peridotite xenoliths, Contrib. Mineral. Petrol. 128 (1997) 228–246.
[71] T. Meisel, R.J. Walker, A.J. Irving, J.-P. Lorand, Osmium isotopic compositions of mantle xenoliths: a global perspective, Geochim. Cosmochim. Acta 65 (2001) 1311–1323.
[72] J. Blichert-Toft, F. Albarède, Lu–Hf isotope geochemistry of chondrites and the evolution of the mantle–crust system, Earth Planet. Sci. Lett. 148 (1997) 243–258.
[73] A.E. Saal, E. Takazawa, F.A. Frey, N. Shimizu, S.R. Hart, Re–Os isotopes in the Horoman Peridotite: evidence for refertilization?, J. Petrol. 42 (2001) 25–37.
[74] G.P. Brey, T. Köhler, Geothermobarometry in four-phase lherzolites II. New thermobarometers, and practical assessment of existing thermobarometers, J. Petrol. 31 (1990) 1353–1378.